Biocatalysis and Agricultural Biotechnology 17 (2019) 352–360

Contents lists available at ScienceDirect

Biocatalysis and Agricultural Biotechnology

journal homepage: www.elsevier.com/locate/bab

Enhancement of thermal imaging by iron oxide nanoparticle – Preliminary study

S.P. Angeline Kirubha*, Alankruti Rajput

Department of Biomedical Engineering, SRM Institute of Science and Technology, Kattnkulathur, Kancheepuram District, 603 203 Tamilnadu, India

ARTICLE INFO

Keywords:
Breast cancer
Thermography
Magnetic nanoparticles
Iron oxide

ABSTRACT

Magnetic nanoparticles (MNP) have been developed in the recent years for various applications like cell separation, immunoassay, and drug delivery. The present study involves the synthesis of stable, biocompatible Iron oxide MNP by coprecipitation of ferric chloride and ferrous chloride with Polyethylene glycol (PEG) as a surfactant to coat the nanoparticles twice. Scanning electron microscopic (SEM) images confirm the formation of uniform MNPs of size 12–17 nm. The peak at 582.2 cm^{-1} in the Fourier transform infrared spectrum (FTIR) corresponds to the Fe–O bond and the peak at 1104.1 cm^{-1} corresponds to a characteristic peak of PEG binding to the iron core. Tumor tissues selectively targeted with MNPs when placed in a magnetic field increases the temperature of the tumor tissues. The phantom study shows that there is a minimum of 1.3 °C and a maximum of 6.7 °C rise in temperature with increasing concentration of the nanoparticles embedded in the phantoms; this proved the possibility of enhancement of thermal images using MNPs and its usage for thermal ablation of cancer. MNPs can also be used as a contrast agent for magnetic resonance imaging (MRI).

1. Introduction

Breast cancer is the second most common cancer in the world and by far the most frequent cancer among women. Breast cancer is the most frequent cancer diagnosed accounting for 23% of the total cancer cases. It is the leading cause of cancer death among females that accounts for 14% of cancer death (Ferlay et al., 2015; Jemal et al., 2011). Early detection of breast cancer can increase the survival chances of the patients. Thermography was proposed more than five decades ago as a cost-effective tool for breast cancer screening (Kennedy et al., 2009; Moore, 2001). The principle of thermography utilizes the difference in skin temperature as a result of carcinoma's presence. Cancerous tissues are well vacuolated thus have an abundant blood supply; as a result, increasing the temperature of the surrounding tissue. Thermal images require an IR camera that captures these temperature differences on the skin surface. These images are then analyzed by the radiologist to detect the thermal patterns that can indicate the presence of an embedded tumor. However thermography has not been accepted as a screening tool for the following reasons: It is difficult to differentiate between natural hot spots and the tumor region, small and deep tumors cannot be identified easily. Ng (2009) suggesting an idea to enhance thermal images to overcome these limitations. There are many attempts to improve the sensitivity and specificity of thermography for early detection of cancer by image processing algorithms (Dinsha and Manikandaprabu, 2014; Koay et al., 2004; Boquete et al., 2012). The proposed study enhances the thermal image by a different approach. In this study, biocompatible Iron Oxide Magnetic nanoparticles (MNP) are synthesized that can be used to target the cancer tissues. These nanoparticles when placed in an electromagnetic field vibrate and thus result in increased temperature and enhances the cancer tissue in the thermal image. These biocompatible magnetic nanoparticles have a broad scope in the field of biotechnology and biomedical engineering. Apart from thermography they can also be used as MRI contrast agents and for targeted thermoablation. A review of each of the breast screening tools and their associated limitations were discussed (Kennedy et al., 2009). No single screening tool provides excellent predictability, but a combination of tools that also incorporates thermography has been shown to boost both sensitivity and specificity. In light of developments in computer technology, anipd the maturation of the Thermographic industry, additional research is required to confirm and continue to develop the potential of this technology to provide a more effective noninvasive adjunctive tool to provide early detection of breast cancer. For the last 1.5 decades of complying with the strict standardized thermogram interpretation protocols by proper infrared trained personnel as documented in the literature, breast thermography has achieved an average sensitivity and specificity of 90%. An abnormal thermogram is reported as the significant biological risk marker for the existence of or continues development of breast tumor. A review paper of thermography discusses the performance and environmental requirements in characterizing

* Corresponding author.
E-mail address: angeline.sp@ktr.srmuniv.ac.in (S.P. Angeline Kirubha).

https://doi.org/10.1016/j.bcab.2018.12.005
Received 21 February 2018; Received in revised form 12 November 2018; Accepted 6 December 2018
Available online 08 December 2018
1878-8181/

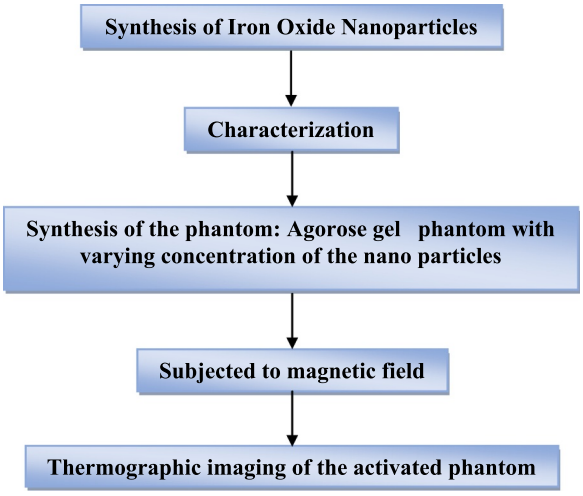

Fig. 1. Overview of the study protocol.

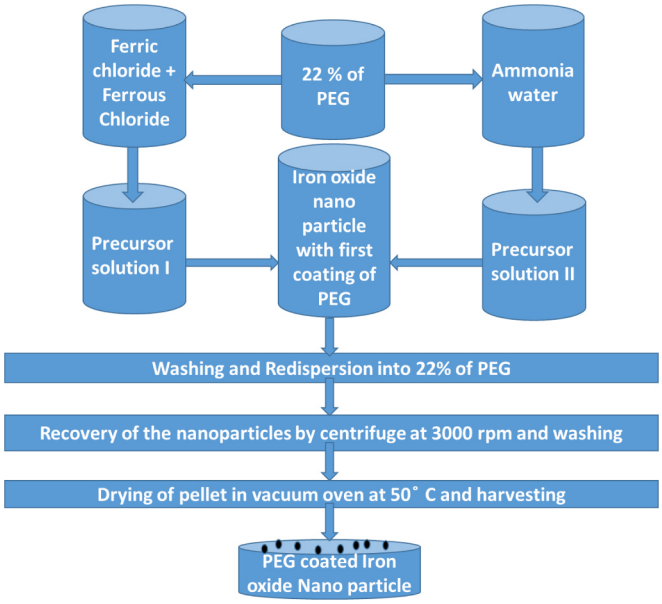

Fig. 2. Synthesis of magnetic nanoparticles by a modified co-precipitation method with the double treatment of surfactant.

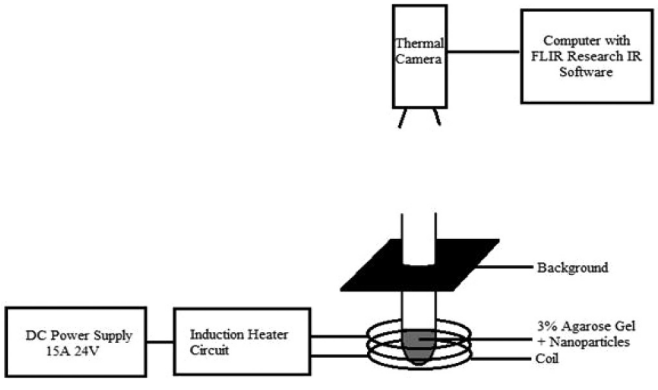

Fig. 3. Experimental set up for dynamic thermal image study.

thermography as being used for breast tumor screening under strict indoor controlled environmental conditions. The article, however, does not preclude users from potential errors and misinterpretations of the data derived from the thermal imager.

Fig. 4. ZVS induction heater.

A new thermography based approach to early detection of cancer using magnetic nanoparticles theory simulation and in vitro validation was proposed by Levy et al. (2010). The author discussed the use of magnetic nanoparticles to enhance thermography signals. Experiments were conducted using an in vitro tissue model, an inductive heating system, and an infrared camera. The thermal images, recorded by the infrared camera during the experiments, were analyzed using an algorithm that was developed as part of this work. The results show that small tumor phantoms (diameter of 0.5 mm) that were embedded under the surface of the tissue phantom (up to 14 mm below the surface) can be detected and located, indicating that the proposed method could potentially offer considerable advantages over conventional thermography and other methods for cancer early detection. Nevertheless, several issues should be clarified in future studies before the method can be offered for clinical use. Dipolar interactions of the bare Fe_3O_4 NPs was found to increase the heating efficiency with increasing particle concentration when placed in a magnetic field (Ihab et al., 2015).

García-Jimeno et al. (2012) proposed the use of magnetic nanoparticles in thermal ablation. Their study shows the temperature increment produced by different concentrations of magnetic nanoparticles inside a phantom, after irradiating tissue mimicking materials (phantoms) with a minimally invasive coaxial antenna working at a frequency of 2.45 GHz. Temperature sensors were placed inside and outside the tumor phantom to assess the focusing effect of heat produced by nanoparticles. Results have shown that the temperature increments depend on the nanoparticles concentration. In this way, a temperature increment of more than 56 ˚C was obtained with a ferrofluid concentration of 13.2 mg/ml, whereas the increase in the reference phantom was only of 21 ˚C

Superparamagnetic iron oxide nanoparticles (SPION) with appropriate surface chemistry have been widely used experimentally for numerous in vivo applications such as magnetic resonance imaging contrast enhancement, tissue repair, immunoassay, detoxification of biological fluids, hyperthermia, drug delivery and in cell separation, etc. Mahmoudi et al. (2011), discussed the synthetic chemistry, fluid stabilization and surface modification of superparamagnetic iron oxide nanoparticles, as well as their usage for biomedical applications.

The surface modifications of magnetic nanoparticles to make them more biocompatible and tumor-specific was discussed by Sezer (2012). Chemical coprecipitation synthesis method of Fe_3O_4 was described by Gupta and Gupta (2005). It illustrates the effect of magnetization and stability based on the surface modification. Shameli et al. (2012) and Ghosh and Bhatkhande (2012) have successfully synthesized Iron Oxide nanoparticles by coprecipitation method. However, their application has not yet been demonstrated.

IONPs can also be used for targeting purpose by conjugating it with the ligands/antibodies specific for receptors/ antigens on the target cells. Coated IONPs have been tagged with Herceptin for targeted delivery to human epidermal growth factor-2 receptor (Her2) and epidermal growth factor receptor (EGFR) overexpressing breast cancer cells. Monoclonal antibodies tagged with Superparamagnetic Iron Oxide Nanoparticle Polymer

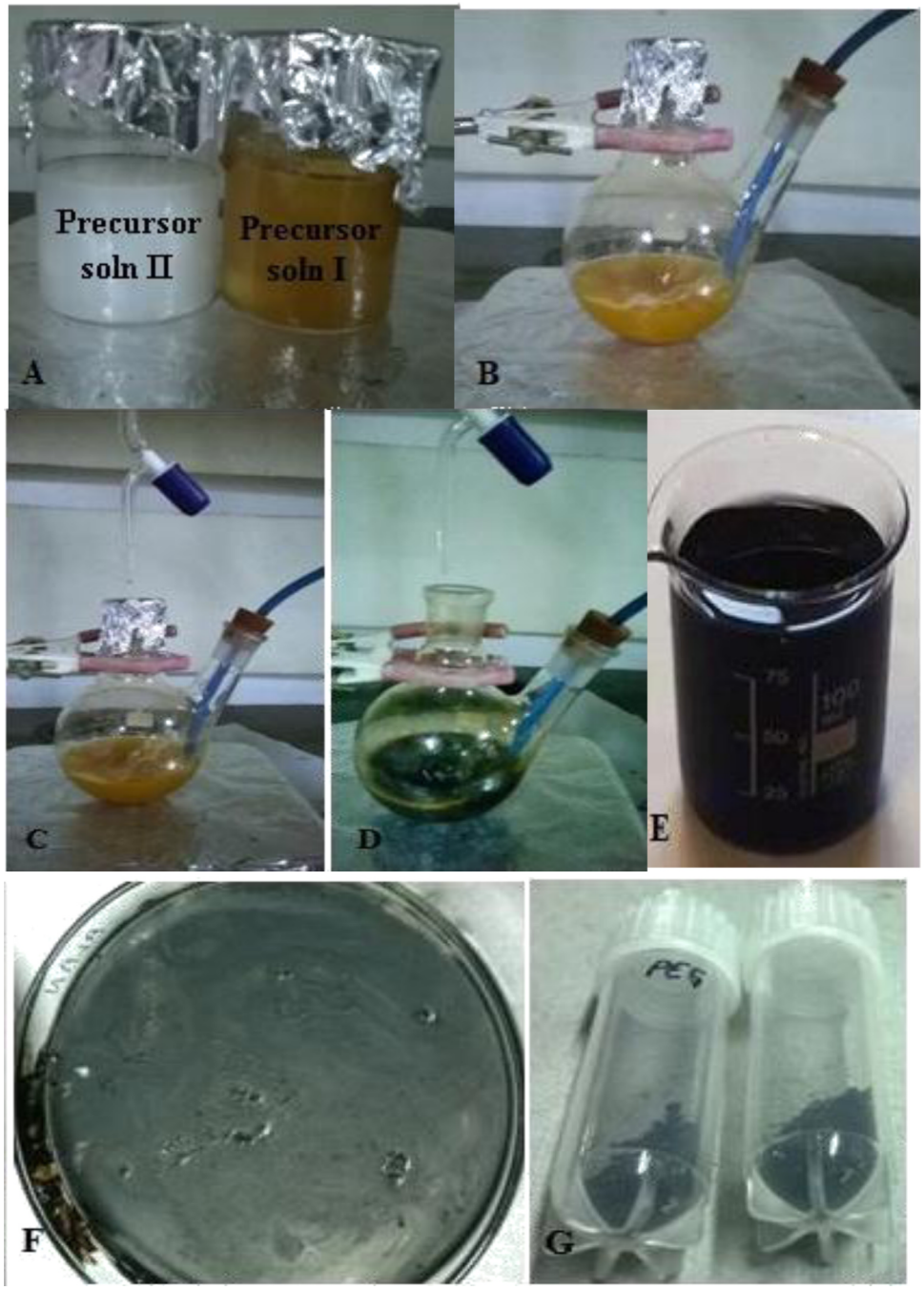

Fig. 5. Synthesis of Iron oxide nanoparticles using the modified coprecipitation method with the double treatment of PEG (A) Prepared precursor solutions II, and I (B) Pretreatment nitrogen gas sparging (C) Dropwise addition of precursor solution II to precursor solution I (D) Change of color of the solution from brown to black. (E) Redispersion of pellet post washing into surfactant solution. (F) Drying of the pellet post washing. (G) Harvested dried sample after grinding in motor and pestle.

helps to target and bind to Phosphatidylserine exposed tumor vessels and increases the accumulation of SPIONPs in breast tumors and enhance tumor contrast (Shivani and Ashu Bhan, 2017). Cell surface nucleolin antagonist, N6L, was used as targeting ligand for MNP by Sader et al. (2015). In vivo biodistribution studies were carried out in MDA-MB 231 tumor-bearing mice, using iron detection assay and proven the targeting of MNP-N6L in the tumor site. Nissim and Robson (1949) and Richter (1959) reported the in vivo biodegradation of iron oxide particles along with the role of ferritin and transferrin in the biodistribution of degradation products. Levy et al. (2010) in his work used 5 mg/ml, γ-Fe_2O_3, mean diameter 20 nm MNPs in an agar gel used as tumor phantom. The author proposed a thermal beacon thermography technique in which the MNPs, located at the tumor site, could be utilized as a "thermal beacon" to detect and locate the tumor by enhancing the thermal images. This study aimed to test the potential of the enhancement of thermography by IONPs by varying the concentration of IONPs in the agar gel.

This paper demonstrates the use of magnetic nanoparticles for enhancement of thermography for diagnosis of cancer in phantom. The objectives of this work are the synthesis of magnetic nanoparticles, then the characterization of the nanoparticles and finally to demonstrate the possible use of the nanoparticles using a phantom study for enhanced thermography.

2. Materials and methods

The overview of the study is illustrated in Fig. 1. The first step is to synthesize the Iron Oxide Nanoparticles. The synthesis was done by

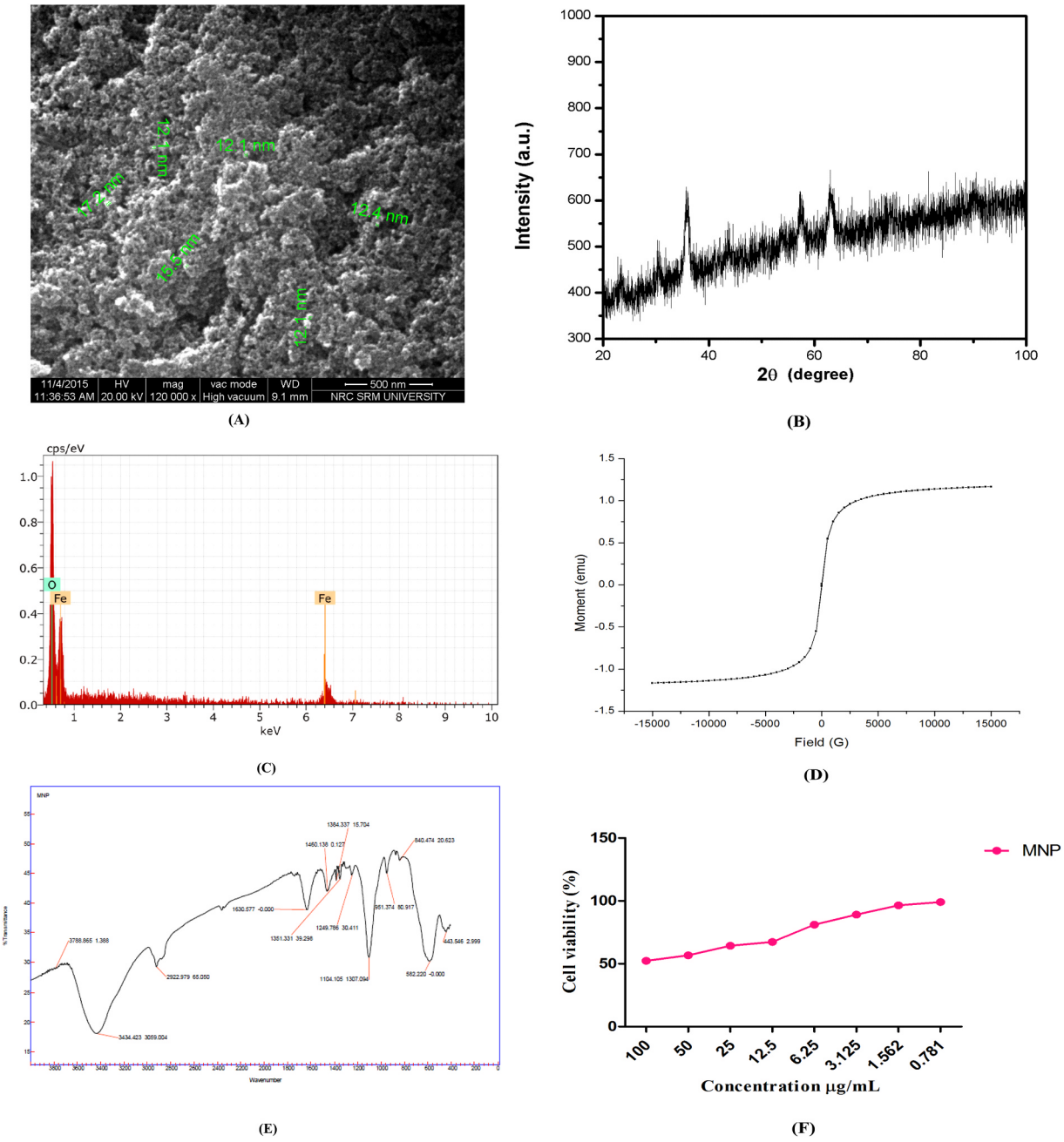

Fig. 6. Characteristics of synthesized Iron oxide nanoparticles (A) SEM image of modified co-precipitation method with double treatment of surfactant (B) XRD spectrum of the magnetic nanoparticles (C) EDS spectrum showing no impurity peaks (D) VSM plot of magnetic moment versus magnetic field strength showing a superparamagnetic curve (E) FTIR spectrum (F) Graph of cell viability versus concentration of nanoparticles.

modifying the well-known coprecipitation method (Laurent et al., 2008; Lee et al., 2004; Sun et al., 2007). The nanoparticles thus developed were then subjected to characterization tests to determine the size, shape, magnetic strength and toxicity of the particles. Once the particles are characterized, they were used in different concentrations for the synthesis of phantoms. These phantoms were synthesized from an agarose gel to mimic the cancer tissue. The developed phantoms are then be subjected to a magnetic field to activate the magnetic nanoparticles. The exposed, activated phantoms were imaged by thermography to assess its utility in cancer detection.

2.1. Methods

2.1.1. Synthesis of iron oxide nanoparticles

The synthesis process is described in Fig. 2. The solution I was prepared by dissolving 1:2 ratio of Ferrous and ferric chloride in distilled water. Solution II with 25% of aqueous Ammonia solution with same quantity as the solution I was taken. With Solution I, and Solution II, 22% of PEG was added to prepare precursor solutions I and II. To create an inert atmosphere for the reaction and to avoid oxidation the precursor solutions were sparged with nitrogen gas.

In inert atmosphere precursor solution II was added dropwise to precursor solution I. The formation of the Magnetite (Fe_3O_4) was indicated by the color change from brown to black by strong stirring at 1000 rpm of the prepared solution for 45 min to complete synthesis of the nanoparticles. The solution was then centrifuged for 10 min to remove the ammonia water at room temperature at 5000 rpm. To remove any trace of ammonia the nanoparticles were redispersed in distilled water and centrifuged again. The process was repeated three times to

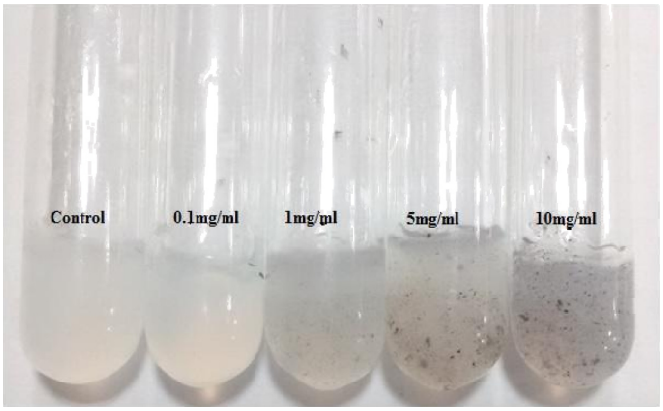

Fig. 7. Phantom: 3% Agarose gel embedded with different concentrations of nanoparticles.

ensure the removal of trace ammonia. The washed nanoparticles were then redispersed into 22% PEG solution for the final coating of the particles. The setup was strongly stirred for 45 mins, followed by centrifugation and washing three times. The nanoparticles were then spread on Petri plate and vacuum dried in the oven at 30 °C overnight. The dried sample was then harvested and ground in a motor and pestle and stored at room temperature (Aranda-Lara et al., 2014; Fitzmaurice et al., 2015).

2.1.1.1. Characterization of iron oxide nanoparticles. Synthesized nanoparticles have been characterized by five tests as explained below. The shape and size of the nanoparticles were determined by Scanning Electron Microscope (SEM). ED pattern provided supports the X-ray Diffraction (XRD) data. Information about the structure of the particles was obtained by Fourier Transform Infrared Spectroscopy (FTIR) and XRD. The magnetic strength of the nanoparticles was estimated by Vibrating Sample Magnetometry (VSM). The cytotoxicity of the particles was carried out to confirm the biocompatibility by the MTT assay.

2.2. Phantom study for dynamic thermal image enhancement

To demonstrate the potential of the nanoparticles to enhance the thermal imaging a phantom study was planned. The phantoms were made of agarose gel and were embedded with Iron oxide nanoparticles synthesized by a modified co-precipitation method with the double treatment of PEG as in the Section 2.2.1. The phantom is then subjected to a magnetic field, and the rise in temperature of the phantom is monitored with dynamic thermal imaging, and the captured thermal images were analyzed for thermal enhancement.

2.2.1. Preparation of the phantom

Studies by Madsen et al. (2005) suggest that 3–4% agarose gel represents tumor tissues (Aranda-Lara et al., 2014). The acoustical wave velocity of carcinoma is 1550 35 m/s, and that of agarose gel representing it is about 1550 7 m/s. Thus, 3% Agarose gel phantom was prepared by measuring the required quantity of Agarose powder and dissolving it in warm distilled water. The required quantity of nanoparticles is then added and mixed. The gel is then allowed to cool and solidify. Different concentrations of the nanoparticles (0 (control), 0.1, 1, 5 and 10 mg/ml) embedded phantoms were prepared.

2.2.2. Experimental setup for dynamic thermal imaging

An overview of the setup is as shown in the Fig. 3. The Induction heating circuit is powered by a DC power supply; this set up is responsible for the alternating magnetic field required to increase the temperature of the nanoparticles. 3% Agarose gel represents tumor. Black cardboard was used as a background to minimize the surrounding disturbance. The thermal camera was placed such that the top view of the test tube could be captured.

2.2.3. Induction heater

Magnetic nanoparticles change spin when placed in a magnetic field; as a result, the magnetic nanoparticles are heated. An induction heating mechanism provides this magnetic field. When an alternating current passes through a coil, the coil creates a magnetic field around it. When the nanoparticles are placed in this magnetic field, it induces a current flow through it just like a transformer. This current is known as eddy current. However eddy current is not the major factor that heats the nanoparticles. The nanoparticles in the magnetic field continuously magnetize and demagnetize causing the particles to heat up due to friction. This phenomenon is known as hysteresis loss. To facilitate the friction, the nanoparticles were suspended in 3% agarose gel. Here, 3% agarose gel was used since it mimics the tumor tissue. To create a magnetic field around the phantom a small ZVS (Zero Voltage Switching) Induction heater flyback driver of 1000 W was used. This induction heating driver shown in Fig. 4 consists of MOSFETs that change the high-frequency DC to pulsating DC. The power source used was 15 A 24 V linear power supply by JED.

2.2.4. Dynamic thermal image acquisition and thermal image analysis

The infrared camera captures the surface thermal profile of objects. The thermal camera FLIR (Forward Looking Infrared) A305SC was used in this study. It has a thermal sensitivity of 0.05 °C, object temperature range of 0 °C to 350 °C and an accuracy of 2 °C. The camera is placed at about 45 cm above from the coil. The set up was prepared as shown in Fig. 4. Different concentrations of the nanoparticles (0, 0.1, 1, 5 and 10 mg/ml) embedded phantoms were taken in separate test tubes and kept inside the inductor coil under magnetic field with a black background. The room temperature was measured and recorded. Using the FLIR Research IR software connected to the thermal camera, thermal videos were taken for two minutes. This experiment was repeated for different phantoms prepared, i.e., control (0), 0.5, 1, 5 and 10 mg/ml of nanoparticles with an interval of one hour between each dynamic image capturing which allows the coil to cool.

From the video a region of interest is selected such that it confines to the region within the test tube. From the region of interest average temperature was measured with respect to time and plotted as the graph of temperature versus time. Percentage change of temperature at 0th second to 120th second was determined using the Eq. (1). Percentage change in temperature corrected with control is determined by the Eq. (2). This is determined for every 10 s, and the average temperature is plotted.

$$\%change\ in\ temperature = \frac{(Temerature\ at\ \ 120^{th}\ \ second - Temerature\ at\ \ 0^{th}\ \ second)}{Temerature\ at\ \ 0^{th}\ \ second} \times 100 \quad (1)$$

$$\%change\ in\ corrected\ temperature = \frac{(Temerature\ of\ sample - Temperature\ of\ control)}{Temperature\ of\ control} \times 100 \quad (2)$$

In real time application, the thermal camera has internal calibration and ADC facilities. So whenever the camera is switched on, both calibration and ADC have been done automatically with respect to the recording room temperature. It takes the digital value of the measured current signal, refers the appropriate calibration curve, and calculates object's surface temperature based on its emission, reflected emission from ambient source, and emission from the atmosphere using the total radiation law. Before the final measurement of surface temperature, suitable correction factors were included due to atmospheric attenuation, reflected ambient temperature, and the camera's ambient temperature drift before the final result is presented.

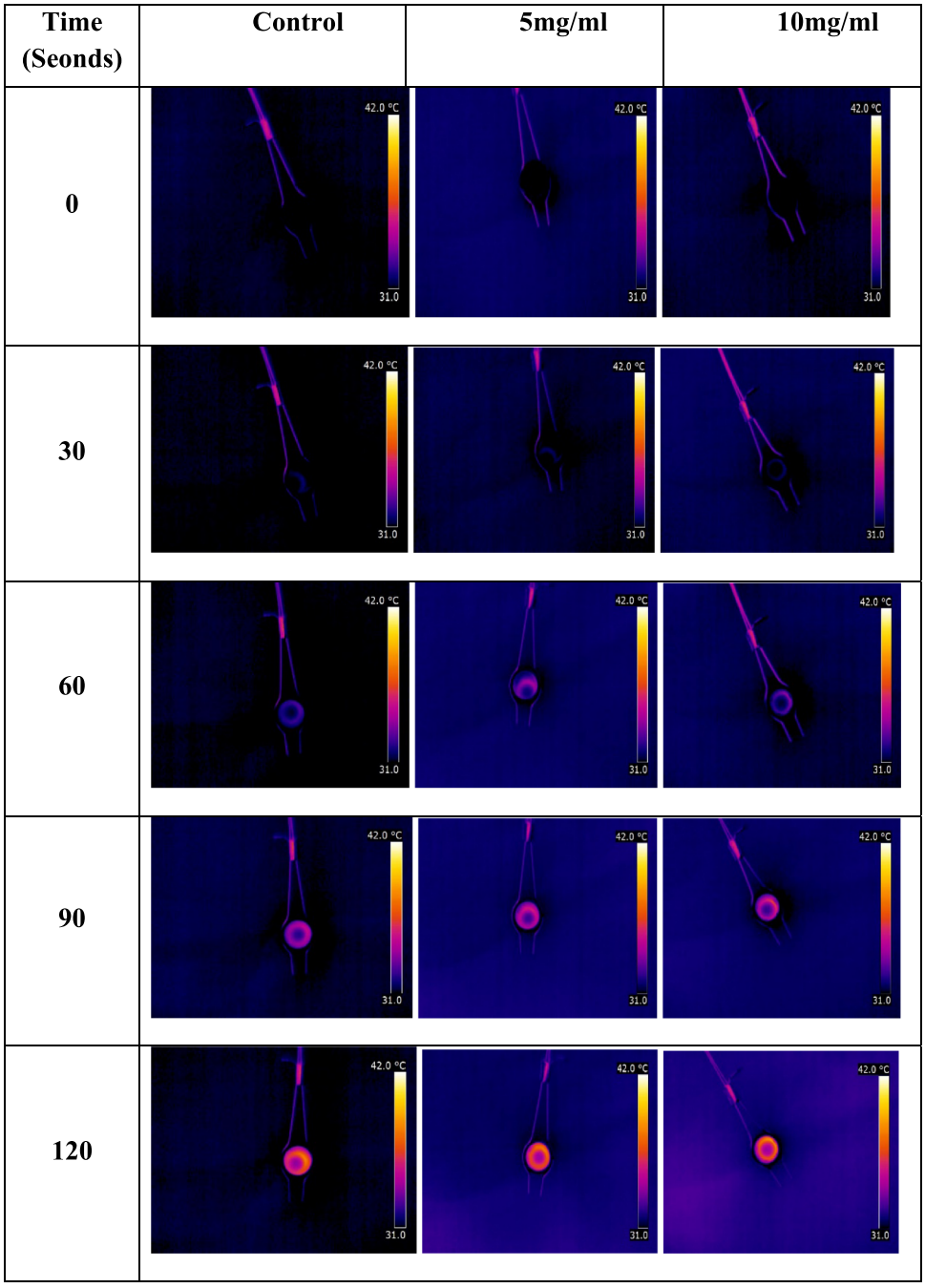

Fig. 8. Comparison of the thermal images of the phantoms of control and phantom with the concentration of 5 mg/ml and 10 mg/ml nanoparticles.

3. Results and discussion

3.1. Synthesis of iron oxide nanoparticles by modified co-precipitation with double treatment of surfactant

Iron oxide nanoparticles were synthesized by the modified co-precipitation with the double treatment of surfactant method as explained in the Section 2.2.1. This method involved a post-treatment with surfactant PEG. After the black precipitate was washed and centrifuged, it was redispersed into 22% PEG Solution. The use of PEG in high concentrations twice increases the cost of the final product. By this method uniformly distributed spherical shaped black colored iron oxide nanoparticle precipitates of size 12–17 nm has been synthesized. Fig. 5 shows the steps involved during the synthesis process.

3.2. Characteristics of synthesized iron oxide nanoparticles

Fig. 6 shows the different characteristics of the synthesized nanoparticles. The size of the nanoparticles was below 20 nm and distributed uniformly as desired and spherical with the mean diameter of 10 nm (Fig. 6. A). The XRD pattern (Fig. 6. B) of the sample proves the purity of the magnetite Sun et al. (2007). It shows that the sample has a cuboidal crystal system. X-ray diffraction pattern analyzed the crystalline structure of iron oxide. (Cu Kα radiation (λ = 0.1548 nm) was applied, and the samples were scanned from 20° to 100° at a scanning rated of 0.5°/min. The phases formed on the surface of iron oxide nanoparticles were investigated using XRD analysis and are illustrated in Fig. 6.A. The XRD patterns of the iron oxide agree with JCPDS#01-075-0449. The major peaks at 35.36°, 30.48°, 43.65° and 79.55° and 39.39° confirm the

Table 1
Change in temperature in the phantom surface measured using dynamic thermal imaging over a period of 2 min.

Relative time (seconds)	Average temperature in specific ROI in each phantom (°C)				
	Control	0.1 mg/ml	1 mg/ml	5 mg/ml	10 mg/ml
0	31.41	31.52	31.41	31.44	31.49
10	31.48	31.48	31.57	31.99	31.99
20	31.70	31.82	31.97	32.63	32.78
30	31.98	32.25	32.40	32.71	32.89
40	32.13	32.67	32.59	33.13	33.43
50	32.78	32.93	33.16	33.39	33.95
60	33.24	33.29	33.62	33.86	34.69
70	33.51	33.71	34.00	34.25	35.77
80	33.78	34.43	34.66	34.72	37.06
90	34.23	35.06	35.23	35.31	38.05
100	34.72	35.70	35.80	35.90	38.64
110	35.35	36.35	36.53	36.67	39.52
120	35.61	36.66	36.91	37.19	41.55
Change in Temperature (°C) after 2 min	4.2	5.14	5.5	5.75	10.06

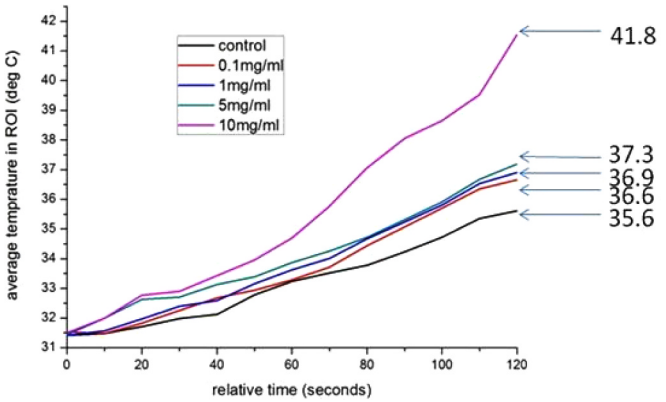

Fig. 9. Change in temperature in the phantoms.

Table 2
Percentage change in temperature in the phantoms with respect to control.

Relative time (seconds)	0.1 mg/ml	1 mg/ml	5 mg/ml	10 mg/ml
0	0.06	0.002	0.09	0.29
10	0.08	0.28	1.63	1.65
20	0.36	0.83	2.92	3.38
30	0.84	1.31	2.29	2.86
40	1.70	1.44	3.13	4.05
50	0.46	1.14	1.83	3.56
60	0.15	1.15	1.88	4.39
70	0.59	1.46	2.20	6.74
80	1.93	2.61	2.77	9.71
90	2.42	2.92	3.15	11.15
100	2.83	3.12	3.41	11.29
110	2.84	3.35	3.76	11.82
120% **Change in Temperature after 2 min**	2.94	3.63	4.44	16.67

presence of the iron oxide. The particle size of the iron oxide was calculated using Sharer's formula, d = 0.9λ / β cosθ; Where, λ wavelength of X-rays, β-FWHM of diffraction peak and θ-angle corresponding to the peaks. The particle size of iron oxide found to be 34.2 nm.

The energy dispersive X-ray spectroscopic pattern (Fig. 6. C doesn't show any impurities. For a mean size of 10 nm, the expected magnetization is 30–35 emu/g. Plot Fig. 6. D indicates the particles have superparamagnetic properties and magnetic susceptibility of about 40 emu/g. If the size of the particles increases, the magnetization also increases. The FTIR Spectra (Fig. 6. D), of the Fe_3O_4 nanoparticles coated with PEG, shows the peak at 3434.4 cm^{-1} is attributed to the stretching vibration of OH ^{1}, which is assigned to OH ^{1} absorption by Fe_3O_4 Nanoparticles. The peak at 582.2 cm^{-1} is attributed to the Fe–O bond vibration of Fe_3O_4. The peak at 2922.98 cm^{-1} belongs to the stretching vibration of OH ^{1}, which represents the stretching vibration of (PEG) $–CH_2$ that is absorbed by Fe_3O_4 Nanoparticles. The peaks at 1460.1 cm^{-1} and 1632.4 cm^{-1} represents a C–H bend and at 1104.1 cm^{-1} represents a C–O stretch of the PEG. Also the O–H bend is attributed to the peak at 951.4 cm^{-1}. MTT assay was conducted for the testing of cell viability. Cell viability percentage was obtained using the equation 3.1 and plotted in the graph (Fig. 6. F.) between the concentrations in g/ml versus cell viability in percentage.

$$\text{Cell viability (\%)} = (\text{Average test optical density} = \text{Controloptical density}) \times 100 \quad (3)$$

3.3. Phantom prepared

Phantoms were prepared with different concentrations of the nanoparticles (0, 0.1, 1, 5, and 10 mg/ml) embedded in 3% of agarose gel. Fig. 7 depicts the phantom prepared.

3.4. Dynamic thermal image acquisition

The experimental set up explained as in section 2.3.2 have been made. The room temperature measured was 31.5 °C. Fig. 8 shows a comparison of the thermal images of the control and 1 mg/ml nanoparticles concentration phantom taken at 10 s interval 0th second to 120th second. The darker shade of blue represents lower temperature while the white represents higher temperatures in the image. From the figure, it is observed that there was a rise in temperature in both the control as well as the test phantom. There is a rise in temperature in the control phantom due to the convection heat generated by the coil. However, due to the presence of nanoparticles in the test, there is a rise in temperature at a faster rate. Table 1 shows the change in temperature every 10 s in the phantoms having different concentrations of nanoparticles, the same was represented in the graph as shown in Fig. 9. As the concentration of nanoparticles in the phantom increases the average surface temperature of the phantom also increases when placed in a magnetic field.

Tables 2 and 3 represents the percentage change in temperature corrected with respect to the control and average respectively. From Table 2, the percentage change in temperature in the phantoms with respect to control after 2 min placed in a magnetic field was found to increase with concentration 2.94, 3.63, 4.44 and 16.67 for phantoms with different concentrations of 0.1, 1, 5 and 10 mg/ml respectively. Fig. 9 represents the graph of the percentage change in temperature

Table 3
Percentage change in temperature in the phantoms with and without correction.

Concentration of nanoparticles	Percentage change in average temperature (without correction)	Percentage change in average temperature (With correction)
Control	5.79	0
0.1 mg/ml	7.16	1.32
1 mg/ml	7.72	1.79
5 mg/ml	8.44	2.58
10 mg/ml	12.79	6.74

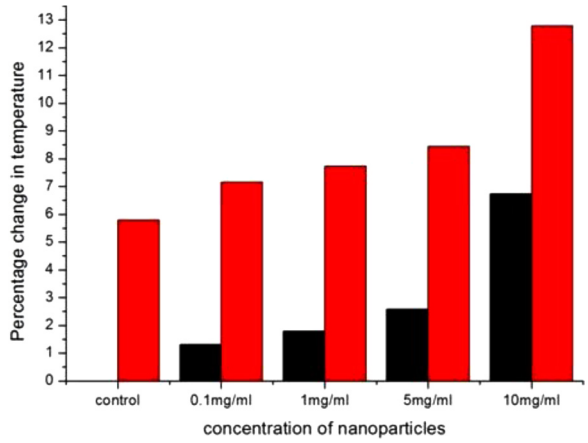

Fig. 10. Percentage change in temperature with and without correction with control.

Table 4
Average temperature of the phantoms in 2 min of exposure to alternating magnetic field.

Concentration of nanoparticles (g/ml)	Average temperature (°C)
Control	35.61
0.1 mg/ml	36.66
1 mg/ml	36.91
5 mg/ml	37.19
10 mg/ml	41.55

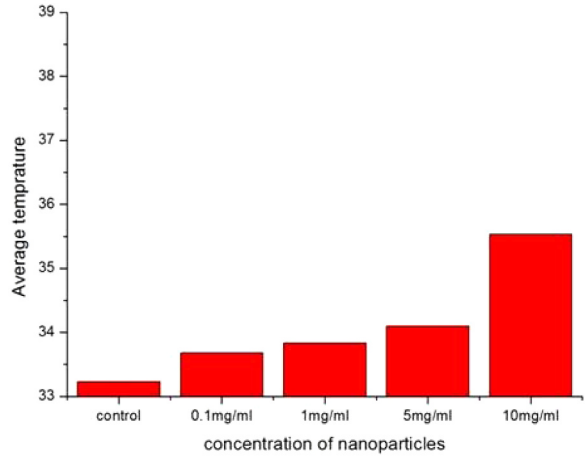

Fig. 11. The average temperature of the phantoms in 2 min of exposure to an alternating magnetic field.

versus time. Fig. 10 shows the comparison between the percentage change in temperature with and without correction with control. The average temperature of the phantoms in two minutes of exposure to the alternating magnetic field was tabulated in Table 4, and the same was plotted as a bar chart in Fig. 11.

From the study, it was found that there is a rise in temperature in control (without nanoparticles) and this is due to the convection heat caused due to the heating of the coil. The maximum temperature attained was 41.8 °C with 10 mg/ml. The average temperature of the different concentration of nanoparticles phantoms in 2 min duration, increases with the increase in concentration. The percentage change in temperature also represents the same. With the experiment conducted we could achieve a minimum rise in temperature of 1.3 °C with 0.1 mg/ml and the maximum of 6.7 °C with 10 mg/ml. These nanoparticles, thus proven that they are suitable to be used for the enhancement of thermography for breast cancer as well as for targeted thermal ablation treatments (Ahmed et al., 2013; Huang and Hainfeld, 2013; Jose Bante-Guerra et al., 2013).

4. Conclusion

Ultrafine, uniform, spherical and highly pure Fe_3O_4 nanoparticles were prepared by modified controlled chemical co-precipitation method from the solution of ferrous/ferric mixed salt solution in aqueous ammonium hydroxide solution with PEG as the chosen surfactant at a concentration of 22%. The use of PEG as a coating surface on the magnetite makes it more biocompatible. The result shows the particle size to be about 10 nm and can be easily dispersed in aqueous solutions for any biomedical application.

The produced magnetic nanoparticles can be used for any biomedical application like magnetic carrier technology, hyperthermia, contrast agents for imaging modalities like MRI and Thermography.

These nanoparticles can be made more specific or targeted by binding to antibodies or other such specific molecules for the increased application. Further, in vivo studies can be used to determine toxicity level and minimum dosage levels required for in vivo applications.

Conflict of interest

No such conflict exists.

References

Ahmed, M., de Rosales, R.T.M., Douek, M., 2013. Preclinical studies of the role of iron oxide magnetic nanoparticles for nonpalpable lesion localization in breast cancer. J. Surg. Res. 185 (1), 27–35.
Aranda-Lara, L., Torres-García, E., Oros-Pantoja, R., 2014. Biological tissue modeling with agar gel phantom for radiation dosimetry of ^{99m}Tc. Open. J. Radiol. 4, 44–52.
Boquete, L., Ortega, S., Miguel-Jiménez, J.M., Rodríguez-Ascariz, J.M., Blanco, R., 2012. Automated detection of breast cancer in thermal infrared images, based on independent component analysis. J. Med. Syst. 36 (1), 103–111.
Dinsha, D., Manikandaprabu, N., 2014. Breast tumor segmentation and classification using SVM and Bayesian from thermogram images. Unique. J. Eng. Adv. Sci. 2 (2), 147–151.
Ferlay, J., Soerjomataram, I., Dikshit, R., Eser, S., Mathers, C., Rebelo, M., Parkin, D.M., Forman, D., Bray, F., 2015. Cancer incidence and mortality worldwide: sources, methods and major patterns in GLOBOCAN 2012. Int. J. Cancer 136 (5), E359–E386.
Fitzmaurice, C., Dicker, D., Pain, A., Hamavid, H., Moradi-Lakeh, M., MacIntyre, M.F., Allen, C., Hansen, G., Woodbrook, R., Wolfe, C., 2015. The global burden of cancer 2013. JAMA Oncol. 1 (4), 505–527.
García-Jimeno, S., Ortega-Palacios, R., Cepeda-Rubio, M.F.J., Vera, A., Salas, L.L., Estelrich, J., 2012. Improved thermal ablation efficacy using magnetic nanoparticles: a study in tumor phantoms. Prog. Electroman. Res. 128, 229–248.
Ghosh, S., Bhatkhande, P., 2012. Encapsulation of PCM for thermo-regulating fabric application. Int. J. Org. Chem. 2 (04), 366.
Gupta, A.K., Gupta, M., 2005. Synthesis and surface engineering of iron oxide nanoparticles for biomedical applications. Biomaterials 26 (18), 3995–4021.
Huang, H.S., Hainfeld, J.F., 2013. Intravenous magnetic nanoparticle cancer hyperthermia. Int. J. Nanomed. 8, 2521–2532.
Ihab, M., Obaidat, Bashar Issa, Yousef, Haik, 2015. Review magnetic properties of magnetic nanoparticles for efficient hyperthermia. Nanomaterials 5, 63–89. https://doi.org/10.3390/nano5010063.
Jemal, A., Bray, F., Center, M., Ferlay, J., Ward, E., Forman, D., 2011. Global cancer statistics. Ca. Cancer J. Clin. 61 (2), 69–90.
Jose Bante- Guerra, MAcias, J.D.L. Caballero-Aguilar, C., Vales - Pinzon, C., Alvarado- Gil, A.A., 2013. Infrared thermography analysis of thermal diffusion induces by RF

magnetic field on agar phantoms loaded with magnetic nanoparticles. In: Proceedings of the SPIE 8584, energy - based Treatment of Tissue and Assessment VII, 858412. ⟨http://dx.doi.org/10.1117/12.2006235⟩.
Kennedy, D.A., Lee, T., Seely, D., 2009. A comparative review of thermography as a breast cancer screening technique. Integr. Cancer Ther. 8 (1), 9–16.
Koay, J., Herry, C., Frize, M., 2004. Analysis of breast thermography with an artificial neural network, Engineering in Medicine and Biology Society, 2004. IEMBS'04, In: Proceedings of the 26th Annual International Conference of the IEEE. pp 1159–1162.
Laurent, S., Forge, D., Port, M., Roch, A., Robic, C., Vander Elst, L., Muller, R.N., 2008. Magnetic iron oxide nanoparticles: synthesis, stabilization, vectorization, physicochemical characterizations, and biological applications. Chem. Rev. 108 (6), 2064–2110.
Lee, S.-J., Jeong, J.-R., Shin, S.-C., Kim, J.-C., Kim, J.-D., 2004. Synthesis and characterization of superparamagnetic maghemite nanoparticles prepared by coprecipitation technique. J. Mag., Magn., Mater. 282, 147–150.
Levy, A., Dayan, A., Ben-David, M., Gannot, I., 2010. A new thermography-based approach to early detection of cancer utilizing magnetic nanoparticles theory simulation and in vitro validation. Nanomedicine:NBM 6 (6), 786–796.
Madsen, E.L., Hobson, M.A., Shi, H., Varghese, T., Frank, G.R., 2005. Tissue-mimicking agar/gelatin materials for use in heterogeneous elastography phantoms. Phys. Med. Biol. 50 (23), 5597.
Mahmoudi, M., Sant, S., Wang, B., Laurent, S., Sen, T., 2011. Superparamagnetic iron oxide nanoparticles (SPIONs): development, surface modification and applications in chemotherapy. Adv. Drug. Deliv. Rev. 63 (1), 24–46.
Moore, S.K., 2001. Better breast cancer detection. IEEE Spectr. 38 (5), 50–54.
Ng, E.-K., 2009. A review of thermography as promising non-invasive detection modality for breast tumor. Int. J. Therm. Sci. 48 (5), 849–859.
Nissim, J.A., Robson, J.M., 1949. Preparation and standardization of saccharated iron oxide for intra venous administration. Lancet 1 (6556), 686–689.
Richter, G.W., 1959. The cellular transformation of injected colloidal iron complexes into ferritin and hemosiderin in experimental animals; a study with the aid of electron microscopy. J. Exp. Med. 109 (2), 197–216.
Sader, M., Couleaud, P., Carpentier, G., Gilles, M.E., Bousserrhine, N., et al., 2015. Functionalization of Iron Oxide Magnetic Nanoparticles With the Multivalent Pseudopeptide N6l for Breast Tumor Targeting. J. Nanomed. Nanotechnol. 6, 299. https://doi.org/10.4172/2157-7439.1000299.
Sezer, A.D., 2012. Recent Advances in Novel Drug Carrier System. InTech, pp. 2012.
Shameli, K., Bin Ahmad, M., Jazayeri, S.D., Sedaghat, S., Shabanzadeh, P., Jahangirian, H., Mahdavi, M., Abdollahi, Y., 2012. Synthesis and characterization of polyethylene glycol mediated silver nanoparticles by the green method. Int. J. Mol. Sci. 13 (6), 6639–6650.
Shivani, Thoidingjam, Ashu Bhan, Tiku, 2017. New developments in breast cancer therapy: role of iron oxide nanoparticles. Adv. Nat. Sci: Nanosci. Nanotechnol. 8, 023002.
Sun, J., Zhou, S., Hou, P., Yang, Y., Weng, J., Li, X., Li, M., 2007. Synthesis and characterization of biocompatible Fe_3O_4 nanoparticles. J. Biomed. Mater. Res. Part A. 80 (2), 333–341.